Monte Carlo Simulations of Na Atoms in Dynamically Disordered Ar Systems: Solid, Liquid, and Critical-Point Fluid Ar

MARIO E. FAJARDO* and JERRY A. BOATZ

Propulsion Directorate/RKS, Phillips Laboratory, Edwards Air Force Base, CA 93524-7680

Received 23 February 1996; accepted 24 May 1996

ABSTRACT

We present the results of simulations of the structures and optical absorption spectra of Na atoms in solid and liquid Ar at its triple point, and in critical-point Ar fluid. The spectral simulations combine a classical Monte Carlo scheme for generating thermally accessible ground state configurations, along with a first-order perturbation theory treatment of the interactions between the excited Na*(3p ^{2}P) atom and the surrounding Ar perturbers [Boatz and Fajardo, *J. Chem. Phys.*, **101**, 3472 (1994)]. These simulations predict a ''triplet'' (i.e., three peaks) absorption lineshape for Na atoms in solid and liquid Ar at its triple point, and an asymmetrical, blue degraded absorption band for Na atoms in critical Ar fluid. We also note and discuss the similarities between the simulated $Na/Ar_{(l)}$ lineshape and an experimental Li/Ar/Xe mixed host matrix spectrum, and the similarities between the simulated spectrum of Na atoms in critical point Ar fluid, and an experimental Li/H_2 matrix absorption spectrum.

Introduction

A recurring issue in the study of metal (M)-atom-doped cryogenic van der Waals solids is the connection between the microscopic structure of the M atom trapping sites and the observed optical spectroscopy of the bulk samples. Experiments have shown that the M atom electronic transitions are perturbed by the matrix environment, with different trapping environments yielding different characteristic spectral signatures.[1] In particular, for M*(P) ← M(S) absorptions, the splitting of the threefold degeneracy of the excited M*(P) state by asymmetries in the local trapping site environment typically results in the so-called ''triplet'' absorption lineshape (i.e., three partially resolved peaks separated by several hundred wave numbers [cm^{-1}]).

Our ultimate goal is to develop a method for predicting *quantitatively* the optical properties of

*Authors to whom all correspondence should be addressed.
E-mail: fajardom@lablink.ple.af.mil

CCC 0192-8651 / 97 / 030381-12

these systems from a knowledge of their microscopic structures and the relevant dynamics. However, the work described in this article is motivated by a more specific question of long standing in the matrix isolation literature: what effects do ''static'' vs. ''dynamic'' asymmetries in the local M atom trapping environment have on the optical absorption lineshape? In this context we use the word ''static'' to describe those structures that persist in a time-averaged sense; for example, the equilibrium positions of the atoms in a solid, whereas by ''dynamic'' we denote geometric fluctuations occurring on the timescale of lattice vibrations (say 10^{-11} to 10^{-13} s). Much of the past discourse over the nature of matrix perturbations has been couched in this language of static vs. dynamic distortions (reviewed in ref. 2, see Introduction and Bibliography).

We recently reported on theoretical simulations of the structures and optical absorption spectra of Na atoms trapped in idealized Ar matrices based on face-centered cubic (fcc) solids, and Na atoms on Ar clusters and solid surfaces.[2] We employed a classical Monte Carlo scheme to generate the absorption spectra as ensemble averages of the $Na^*(3p\,^2P) \leftarrow Na\ (3s\,^2S)$ transition energies calculated using a degenerate first-order perturbation theory treatment[3,4] of the $Na^*(3p\,^2P)$ excited states. This level of approximation yielded qualitative agreement with the experimentally observed lineshapes. The main results from that study were: (1) trapping sites in which the equilibrium positions of the nearest neighbor Ar atoms exhibit high symmetry (e.g., the O_h one-atom substitutional and T_d four-atom substitutional sites in fcc Ar) yield the experimentally well known ''triplet'' lineshape; (2) trapping environments with equilibrium structures of lower symmetry possessing a single strongly preferred axis (e.g., the C_{2v} two-atom substitutional site, or any surface site) yield a widely separated ''doublet plus singlet'' lineshape; and (3) trapping sites with only minor deviations from a highly symmetrical equilibrium structure can yield a narrowly separated doublet plus singlet pattern at low temperatures and a symmetrical triplet pattern at higher temperatures. Thus, we concluded that, for Na atoms trapped in the O_h or T_d (multi)substitutional sites, the appearance of the triplet absorption is due solely to ''dynamic distortions''[5] of the trapping site, and that the doublet plus singlet pattern appears to be diagnostic of strong, permanent, axial asymmetries in the trapping environment. The third class of sites, for which elevating the temperature gives a qualitative change in the absorption lineshape, are cases in which the dynamic geometry fluctuations eventually wash out the original mild static asymmetries to yield the classic triplet lineshape.

We also recently reported the results of experiments on the $(2p\,^2P) \leftarrow (2s\,^2S)$ optical absorptions of Li atoms trapped in pure Ar, pure Xe, and mixed Ar/Xe host matrices.[6] We hoped that changing the matrix host composition would vary the degree of static disorder in the solid, and that changing the temperature would independently vary the magnitude of dynamic distortions in a given sample. We naively expected that extensive inhomogeneous broadening of the impurity Li-atom transitions in the concentrated rare gas alloys would result in a broad featureless ''lump'' absorption lineshape. Surprisingly, the absorption lineshape changed smoothly with matrix host composition, and a triplet-like feature persisted at all matrix compositions! The splitting between the outermost peaks of the triplets increased from about 700 cm^{-1} in pure Ar, to about 1300 cm^{-1} in the 50/50 Ar/Xe host, and diminished to 560 cm^{-1} in pure Xe (all at $T = 20$ K). The Li-atom absorption exhibited a very weak temperature dependence over the $T = 10$ K to 50 K range in the mixed host matrices, in contrast to the well-known and dramatic effects of temperature on lineshapes in the pure host matrices. This weak dependence is consistent with our picture of these mixed host matrices as amorphous, or at least substitutionally disordered, materials—shaking up an already highly statically disordered system results in very little additional line broadening or splitting.

At this point we would like to apply the theoretical methods used in ref. 2 directly to the problem of (P) ← (S) transitions of M atoms in hypothetical statically disordered rare gas (Rg) matrices. However, our main approach for generating these trial disordered low temperature structures (i.e., quenching of higher temperature dynamically disordered M/Rg systems[7]) requires us to first examine how our methods work on ''fluid'' Rg systems. We are particularly concerned about possible artifacts in the calculations (e.g., finite size/periodic boundary condition effects[8]) which may unphysically bias the systems during the quenching process. We are also interested in investigating these fluid systems in their own right, eventually comparing those results from highly dynamically disordered systems with experiments and simulations of amorphous solid systems. Thus, in this study we will further focus our attention to simu-

lations of Na/Ar systems at higher temperatures, with temperatures and densities corresponding to: (1) solid Ar at its triple point; (2) liquid Ar at its triple point; and (3) Ar fluid at its critical point.

In what follows, we will briefly describe our theoretical model of the absorption lineshapes of M/Rg systems, directing the interested reader to ref. 2 for more details. We will spend a little more time describing the specifics of our computer code implementation of this model, and our strategies for assessing the importance of any artifacts in the simulations. We will find and describe the expected structural artifacts, and show that the present lineshape simulations are very *insensitive* to their presence. These simulations result in our prediction of a triplet absorption lineshape for Na atoms in liquid Ar, a medium in which M atoms might someday be shown to exist as metastable transient species, in analogy to the impurity-atom-doped liquid helium II systems of great current interest.[9] We will also find that the simulated $Na/Ar_{(l)}$ absorption lineshape is very similar to that observed experimentally for Li atoms in mixed Ar/Xe hosts, and that the simulated lineshape for Na atoms in Ar at its critical point qualitatively resembles the experimental spectrum of Li atoms trapped in ''quantum solid'' molecular H_2 matrices.[10] We will discuss the implications of these similarties to both our understanding of M/Rg systems, and to our plans for future simulations.

Theory and Methodology

LINESHAPE EXPRESSION

We have previously described and discussed[2] the theoretical foundations of our lineshape simulation method, and will only repeat a few salient aspects here. We use the ''classical Franck–Condon principle'' expression for the condensed phase absorption lineshape[11]:

$$I(\omega) \propto \sum_i \sum_f p_i \left|\overline{\mu_{fi}^{el}}\right|^2 \int d\mathbf{Q}\, \mathscr{P}_i(\mathbf{Q}) \times \delta\left[\left(E_f(\mathbf{Q}) - E_i(\mathbf{Q})\right)/\hbar - \omega\right] \quad (1)$$

where p_i is the population of the initial electronic state; $\overline{\mu_{fi}^{el}}$ is the electronic transition moment coupling the initial and final electronic states, averaged over the nuclear coordinates, $\mathbf{Q}$; $\mathscr{P}_i(\mathbf{Q})$ is the classical statistical mechanical probability distribution for the initial electronic state; and $E_i(\mathbf{Q})$ and $E_f(\mathbf{Q})$ are the energies of the system at configuration $\mathbf{Q}$ in the initial and final electronic states, respectively.

ENERGY EVALUATION

We estimate $E_i(\mathbf{Q})$ as a pairwise sum over the diatomic (Ar–Ar and Na–Ar) ground-state potentials, and employ a simple yet elegant approximation for $E_f(\mathbf{Q})$ based on first-order degenerate perturbation theory,[3,4] which relates the excited state energy back to the excited Na*(3p)–Ar and ground state Ar–Ar pair potentials. Briefly, the eigenvalues, E, of the total Hamiltonian for the Na-atom optically active electron are obtained by solving:

$$\det\left|V_{\alpha\beta} - (E - \varepsilon_\alpha)\delta_{\alpha\beta}\right| = 0 \quad (2)$$

where:

$$V_{\alpha\beta} = \sum_k \langle\, \chi_\alpha(\vec{\mathbf{r}}) \left| V\left(\vec{\mathbf{r}}, \vec{\mathbf{R}}_k\right) \right| \chi_\beta(\vec{\mathbf{r}})\rangle \quad (3)$$

$V(\vec{\mathbf{r}}, \vec{\mathbf{R}}_k)$ is perturbation due to the kth Ar atom; $\vec{\mathbf{r}}$ and $\vec{\mathbf{R}}_k$ are the electronic and nuclear coordinates, respectively; and the eigenvalues and eigenfunctions of the unperturbed Hamiltonian are denoted by ε_α and $\chi_\alpha(\vec{\mathbf{r}})$, respectively. We ignore the 17.2 cm^{-1} spin-orbit splitting of the excited Na atom 3p state,[14] and the basis set $\{\chi_\alpha\}$ is restricted to the three free-atom states: $\{3p_{-1}, 3p_0, 3p_1\}$. For this basis set, the perturbation matrix becomes:

$$\underline{\underline{\mathbf{V}}} = \sum_k \left(\langle V_0(R_k)\rangle \underline{\underline{\mathbf{I}}} + \frac{1}{10}\langle V_2(R_k)\rangle \times \begin{Bmatrix} -(3\cos^2\theta_k - 1) & -3\sqrt{2}\sin\theta_k\cos\theta_k e^{-i\phi_k} & -3\sin^2\theta_k e^{-2i\phi_k} \\ -3\sqrt{2}\sin\theta_k\cos\theta_k e^{i\phi_k} & 2(3\cos^2\theta_k - 1) & 3\sqrt{2}\sin\theta_k\cos\theta_k e^{-i\phi_k} \\ -3\sin^2\theta_k e^{2i\phi_k} & 3\sqrt{2}\sin\theta_k\cos\theta_k e^{i\phi_k} & -(3\cos^2\theta_k - 1) \end{Bmatrix} \right) \quad (4)$$

where the distance-dependent matrix elements are related to the diatomic pair potentials by[15–17]:

$$\langle V_0(R_k)\rangle \equiv \langle \chi_\alpha(r)|V_0(r, R_k)|\chi_\beta(r)\rangle = \tfrac{1}{3}(V_{B\Sigma}(R_k) + 2V_{A\Pi}(R_k)) \quad (5a)$$

$$\langle V_2(R_k)\rangle \equiv \langle \chi_\alpha(r)|V_2(r, R_k)|\chi_\beta(r)\rangle = \tfrac{5}{3}(V_{B\Sigma}(R_k) - V_{A\Pi}(R_k)) \quad (5b)$$

Eq. (2) will yield up to three distinct energies, E, which represent the contribution to the total energy due to the electronic excitation and the M*–Rg interactions. Because the Na/Ar $S \rightarrow P$ transition energies are calculated as the difference between final and initial state energies, the initial and final state Ar–Ar interactions cancel exactly.

Plots of the Ar–Ar ground-state potential (HFD-B2, ref. 12), and the Na–Ar ($X^2\Sigma$), ($A^2\Pi$), and $B^2\Sigma$) potentials (ref. 13) used in these simulations are shown in Figure 1 of ref. 2. We set the asymptotic energy of the excited Na*–Ar potentials to 16968 cm^{-1}, the weighted average of the energies of the Na*($3p\ ^2P_{1/2}$) and ($3p\ ^2P_{3/2}$) states,[14] and ignore the effects of spin-orbit coupling throughout the simulations.

SIMULATION TECHNIQUES

We perform the integration over initial state configurations specified in eq. (1) by a classical Monte Carlo (MC) simulation scheme based on the original Metropolis algorithm.[18] The absorption lineshapes are calculated as histograms by generating a pseudo-random sequence of thermally accessible configurations and binning the transition energies defined by the delta function in eq. (1), with a resolution of 20 cm^{-1}.

Along with the absorption lineshape, we simultaneously calculate the Na–Ar radial distribution function, RDF or "$g(R)$," which measures the probability of finding an Ar atom at a given distance from the Na atom, relative to the same probability calculated for an ideal gas at the same density.[19] Binning the Na–Ar distances actually yields directly the Na–Ar radial *probability* distribution function (RPDF), which we have reported on exclusively in our previous works on solid systems.[2, 20]

We also generate an angular probability distribution function, $F(\theta, \phi)$, where the polar and azimuthal angles (θ, and ϕ, respectively) of the Ar atoms are calculated in a coordinate system centered on the Na atom. This $F(\theta, \phi)$ only includes contributions from "first nearest neighbor" Ar atoms; that is, those Ar atoms with distances of between 3.0 and 5.0 Å from the Na atom. We adopt the convention that $F(\theta, \phi)$ is constant for an isotropic fluid, thus the total number of Ar atoms between 3.0 to 5.0 Å from the Na atom is given by $\int\int F(\theta, \phi)\sin(\theta)\ d\theta\, d\phi$. We use both $g(R)$ and $F(\theta, \phi)$ to help diagnose the presence of finite-size artifacts in our simulations.

Each simulation begins with an initial configuration of the Na atom and its Ar perturbers based on an fcc Ar lattice, expanded isotropically to yield

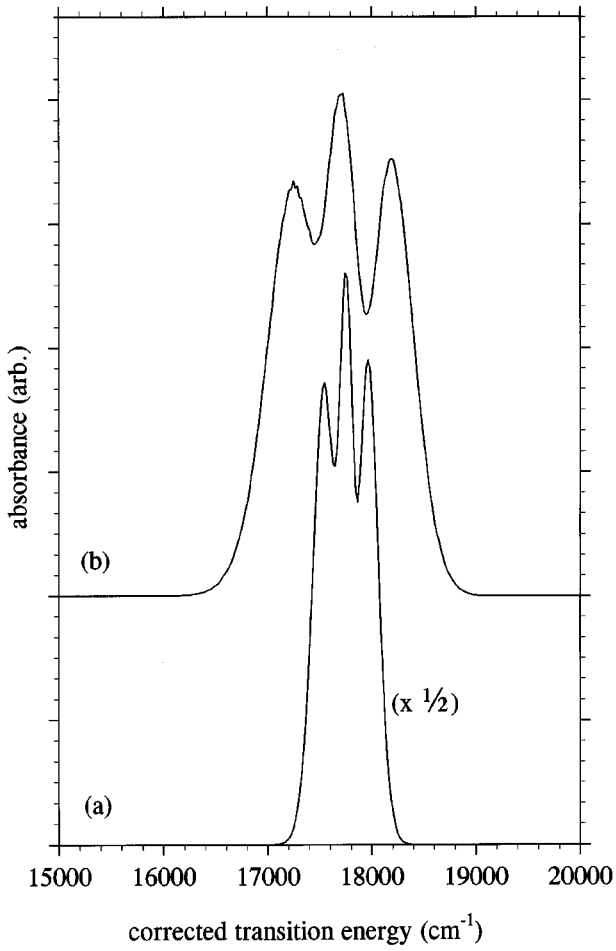

FIGURE 1. Simulated 3p ← 3s absorption spectra for a Na atom in single substitutional sites in solid fcc Ar at (a) $T = 20$ K and (b) $T = 84$ K. The data in (a) have been multiplied by a factor of 1/2 for ease of presentation. The ensembles consist of one Na atom and 107 Ar atoms with three-dimensional periodic boundary conditions constraining the volumes to those normally occupied by 108 Ar atoms. The data in (a) were averaged over 1.7×10^6 configurations, those in (b) over 1.0×10^6 configurations.

the appropriate net atomic number density for the system under study. An initial ''warmup'' period, in which each atom is given $\sim 10^4$ opportunities to hop, is used to encourage equilibration of the ensemble before accumulation of the histograms. We used three different size cubical ''cells'' in these simulations: a $4 \times 4 \times 4$ collection of (100) planes containing 32 total atoms; a $6 \times 6 \times 6$ plane ensemble totaling 108 atoms; and an $8 \times 8 \times 8$ plane system totaling 256 atoms. Three-dimensional periodic boundary conditions with the ''minimum image convention'' were used to simulate infinite systems.[19, 21] All interaction potentials and calculations of spectral and structural properties were truncated for atomic separations greater than half the length of a cell edge.

We also experimental briefly with eliminating the periodic boundary conditions altogether by placing an ensemble of 141 atoms (to include the first eight ''shells'' in an fcc structure) in a rigid spherical box. These simulations were part of our effort to identify and alter any artifacts introduced by our use of periodic boundary conditions. At temperatures and densities corresponding to liquid Ar, the initially centrally located Na atom would quickly find its way to the box wall, where it would subsequently remain (this geometry minimizes the number of Na–Ar interactions, which are less energetically favorable than Ar–Ar interactions). This situation required a procedure for repeatedly recentering the Na atom. We settled on swapping the position of the Na atom with that of the Ar atom closest to the box center, whenever the Na atom hopped to a position more than halfway from the box center to the box wall. This swap was then followed by a short re-equilibration period during which accumulation of ensemble averages was suspended. On average, the Na atom would ''diffuse'' the $\approx$ 5-Å distance in about 5000 attempted hops of 0.3-Å maximum length each. Each atom in the ensemble makes 100 attempts to hop following each recentering event before resumption of the averaging processes. However, several obvious artifacts of the recentering process persist in the data (vide infra) which, at least, are qualitatively different from those introduced by the use of periodic boundary conditions.

LONG-RANGE CORRECTIONS

Our potential truncation scheme requires the use of consistent long-range corrections to the calculated transition energies. In ref. 2 we showed how, within our simple first-order model, the gas-to-matrix energy shift of the centroid of the absorption band is independent of the angular arrangement of the Ar perturbers around the Na atom. In fact, the shift is given by a simple summation over Na–Ar pairs of the so-called ''difference potential'' between the spherical average of the excited Na*–Ar interactions and the ground-state Na–Ar ($X\,^2\Sigma$) diatomic potential (see ref. 2: eq. (10) and Fig. 1c). Thus, the missing long-range contributions to the centroid shift, ΔE_{corr}, can be estimated by integration of the difference potential, $V_{\mathrm{shift}}(R)$, over a constant density continuum of perturbers:

$$\Delta E_{\mathrm{corr}} = 4\pi\rho_{\mathrm{Ar}} \int_{R_{\mathrm{cutoff}}}^{\infty} V_{\mathrm{shift}}(R)\, R^2\, dR \qquad (6)$$

TABLE I.
Summary of Long-Range Transition Energy Correction Factors Used in This Study.[a]

Ensemble, systems simulated	T(K)	ρ_{Ar} (g / cm^3)	R_{cutoff}(Å)	ΔE_{corr}(cm^{-1})
32-atom fcc $4 \times 4 \times 4$ cell				
Ar liquid	84	1.416	5.72	−245
108-atom fcc $6 \times 6 \times 6$ cell				
Ar solid	20	1.764	7.97	−215
Ar solid	84	1.623	8.20	−175
Ar liquid	84	1.416	8.58	−130
Ar fluid	150	0.529	11.92	−10
256-atom fcc $8 \times 8 \times 8$ cell				
Ar liquid	84	1.416	11.44	−25
141-atom rigid spherical box				
Ar liquid	84	1.416	11.64	−25

[a] Values of ΔE_{corr} are rounded to the nearest 5 cm^{-1}. The densities of the Ar solids are taken from ref. 22, the other densities are from ref. 23.

TABLE II.
Summary of Optical Absorption Peaks Calculated in This Study.[a]

Ensemble, systems simulated	Absorption peak energies (cm^{-1})	Peak shifts from free Na atom (cm^{-1})	Centroid shift (cm^{-1})
32-atom fcc 4 × 4 × 4 cell			
Ar liquid, T = 84 K	17155, 17675, 18355	+185, +705, +1385	+730
108-atom fcc 6 × 6 × 6 cell			
Ar solid, T = 20 K	17545, 17745, 17965	+575, +775, +995	+780
Ar solid, T = 84 K	17245, 17705, 18185	+275, +735, +1215	+725
Ar liquid, T = 84 K	17050, 17530, 18190	+80, +560, +1220	+600
Ar fluid, T = 150 K	16830, 17650sh	−140, +680sh	+175
256-atom fcc 8 × 8 × 8 cell			
Ar liquid, T = 84 K	17015, 17495, 18115	+45, +525, +1145	+560
141-atom rigid spherical box			
Ar liquid, T = 84 K	17155, 17735, 18395	+185, +765, +1425	+775

[a]All energies include the long-range corrections listed in Table I, and are rounded to the nearest 5 cm^{-1}.
sh = shoulder.

This estimate is only as good as the assumption of constant density [i.e., constant $g(R)$] implicit in eq. (6); the reader should note that this assumption is particularly bad for the $Na/Ar_{(l)}$ simulations employing the 32-atom 4 × 4 × 4 cell in which the R_{cutoff} is actually less than the typical distance from the Na atom to the second solvation shell of Ar atoms. Table I includes a summary of the bulk Ar densities (ρ_{Ar}), truncation distances (R_{cutoff}), and long-range energy corrections used in the simulations.

Results

Na atom in solid Ar

Figure 1 shows the simulated $Na^*(3p\ ^2P) \leftarrow Na(3s\ ^2S)$ absorption lineshapes for Na atoms trapped in single substitutional sites in solid fcc Ar at T = 20 K, and T = 84 K, calculated using the 108 atom ensembles. The spectra show the classic triplet absorption feature we have come to expect[2] for dynamically distorted trapping sites with highly symmetrical equilibrium structures; the positions of the absorption peaks are included in Table II.

Figure 2 shows the Na−Ar RDFs, and Figure 3 shows the angular probability distributions, from the same simulations as described for Figure 1. The positions of the peaks in the RDFs, and in the $F(\theta, \phi)$, are characteristic of the octahedral single substitutional fcc site,[20] with a minor radial expansion of the first nearest neighbor Ar shell relative to fcc solid Ar.

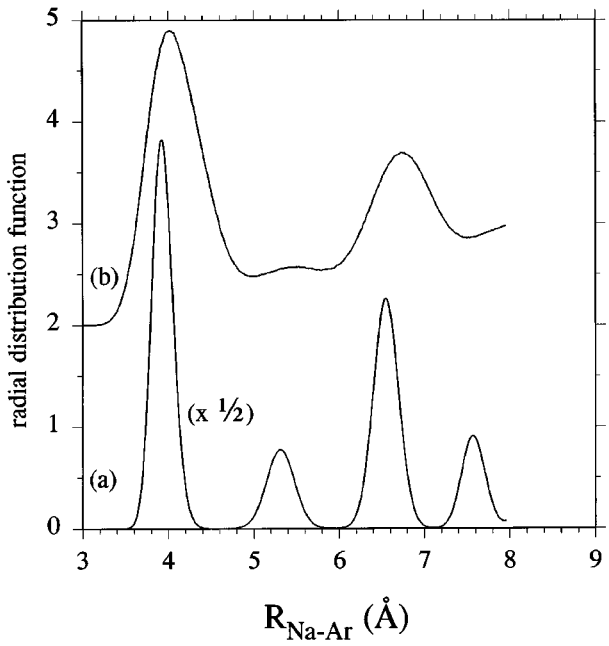

FIGURE 2. Simulated Na−Ar RDFs for a Na atom in single substitutional sites in solid Ar at (a) T = 20 K and (b) T = 84 K; ensembles and simulation parameters as described for Figure 1. The data in (a) have been multiplied by a factor of 1 / 2 for ease of presentation.

Na atom in liquid Ar

Figure 4 shows the simulated $Na^*(3p\ ^2P) \leftarrow Na(3s\ ^2S)$ absorption lineshapes for Na atoms in liquid Ar at T = 84 K, calculated using a variety of ensembles; the absorption peaks are reported in Table II. The spectra all clearly show an obvious triplet absorption pattern, and many other similar-

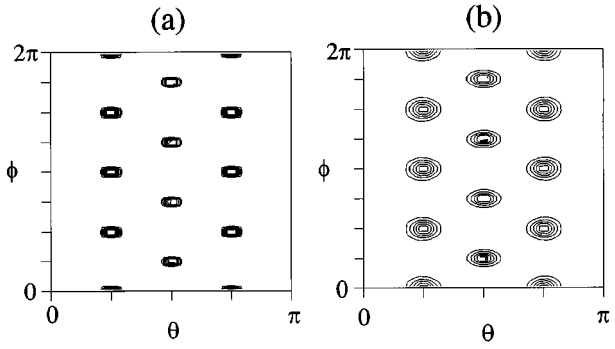

FIGURE 3. Contour plots of simulated angular distribution functions, $F(\theta, \phi)$, of nearest neighbor Ar atoms around a Na atom in single substitutional sites in solid Ar at (a) $T = 20$ K and (b) $T = 84$ K; ensembles and simulation parameters as described for Figure 1. The contours correspond to a range of $F(\theta, \phi)$ values in trace (a) of 0 to 35 in increments of 5, and in trace (b) of 0 to 12 in increments of 2. Contributions from ''second nearest neighbor'' Ar atoms approaching within 5 Å of the Na atom have been deliberately excluded.

ities which are remarkable, given the differences in the simulated structures evident in Figure 5, which shows the Na–Ar RDFs, and in Figure 6, which shows the angular probability distributions. For example, the RDFs calculated using the 108-, 256-, and 32-atom fcc boundary ensembles (Fig. 5a–c) all peak first near 4.75 Å, however, with respective peak heights of 1.85, 1.75, and 1.98. Also, the RDF for the 141-atom ensemble shown in Figure 5d exhibits gross distortions, probably due to incomplete equilibration following the recentering events, and to the use of a rigid spherical boundary; however, all the simulated spectra are very similar. Also, qualitative examination of the angular distributions in Figure 6 reveals obvious finite size artifacts (especially Fig. 6c) which do not seem to have any dramatic effect on the calculated lineshapes.

We also performed a short series of simulations to determine the effects of removing one or several Ar atoms, from the immediate vicinity of the Na atom, in the initially 108-atom fcc boundary ensemble. For low-temperature Na/Ar solids, we showed that this procedure leads to a family of hypothetical relaxed trapping sites with very different local structures and absorption lineshapes.[2] Figure 7 shows that, at the present higher temperatures and lower densities, removing additional Ar atoms apparently just results in a further reduction of the density of the Ar liquid, which is manifested in the spectra primarily as a reduced blue shift

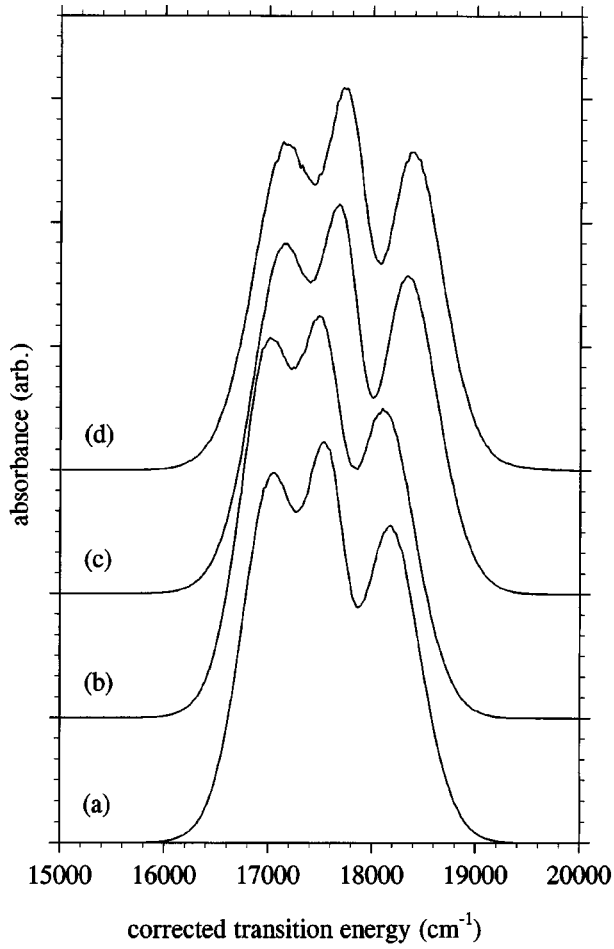

FIGURE 4. Simulated 3p ← 3s absorption spectra for a Na atom in liquid Ar at $T = 84$ K, calculated using four different ensembles: (a) the 108-atom, $6 \times 6 \times 6$ (100) plane assembly with fcc periodic boundary conditions; (b) the 256-atom, $8 \times 8 \times 8$ plane fcc; (c) the 32-atom, $4 \times 4 \times 4$ plane fcc; and (d) the 141-atom collection in a rigid spherical box of radius 11.64 Å. The number of configurations averaged over for each simulation were: (a) 2.0×10^6; (b) 1.9×10^6; (c) 5.0×10^6; and (d) 1.0×10^6.

from the gas phase transition energy. Eventually, reducing the density of perturbers around the Na atom does change the lineshape from a more or less symmetrical triplet to an asymmetrical, blue-degraded, doublet-plus-singlet pattern; see Figure 7f. The continuation of that trend will become apparent in the following section.

Na Atom in Ar Fluid at its Critical Point

Figure 8 shows the simulated Na*(3p ^{2}P) ← Na (3s ^{2}S) absorption lineshape for a Na atom in Ar

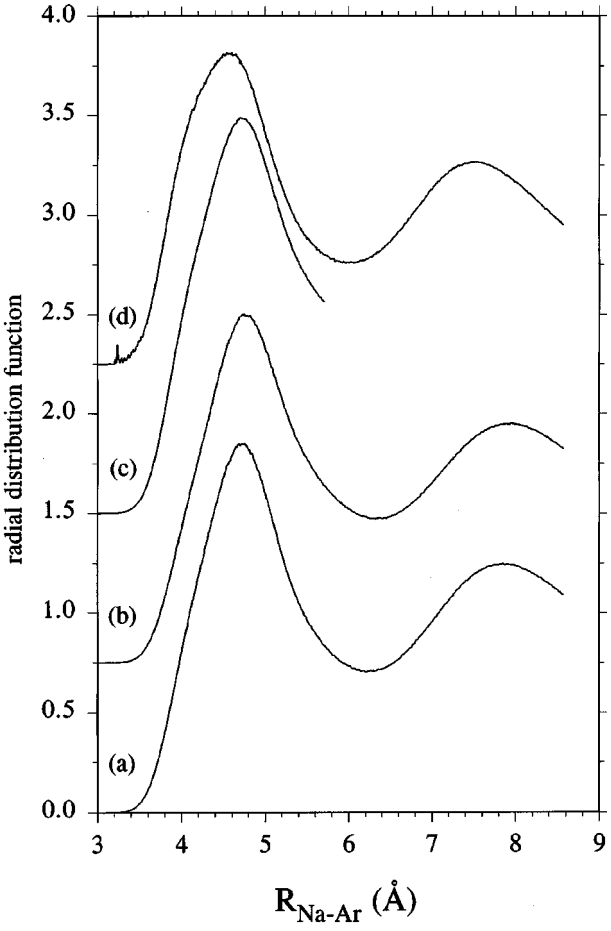

FIGURE 5. Simulated Na–Ar RDFs for a Na atom in liquid Ar at $T = 84$ K; ensembles and simulation parameters as described for Figure 4. The small spikes in trace (d) between 3 and 4 Å are artifacts of the Na atom ''recentering'' process described in the text.

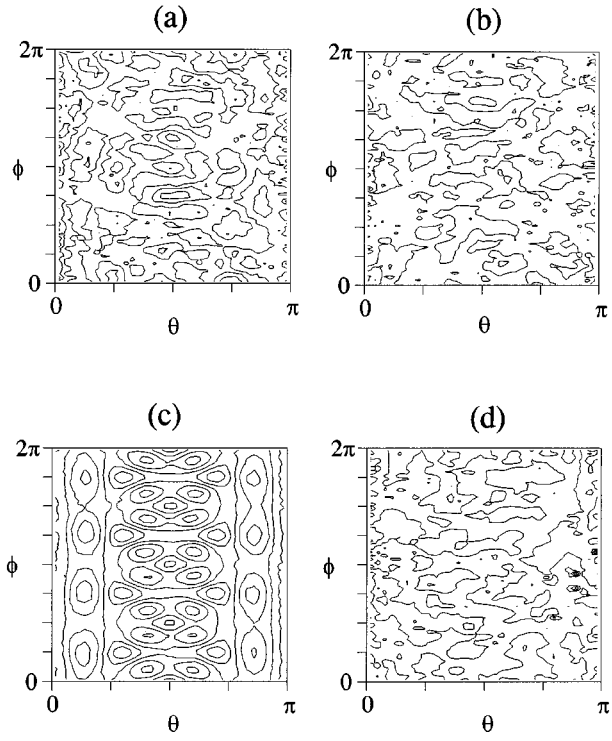

FIGURE 6. Contour plots of simulated angular distribution functions, $F(\theta, \phi)$, of ''nearest neighbor'' Ar atoms around a Na atom in liquid Ar at $T = 84$ K; ensembles and simulation parameters as described for Figure 4. The $F(\theta, \phi)$ contour ranges and increments are: (a) 0.6 to 0.9; step 0.05; (b) 0.55 to 0.8 step 0.05; (c) 0.3 to 1.2 step 0.15; and (d) 0.6 to 1.3 step 0.1.

fluid at its critical point density and at $T = 150$ K, calculated using the 108-atom ensemble. The spectrum shows a sharp peak slightly red shifted from the free Na-atom transition energy and a broad shoulder extending to higher energies, which is very different from the previously described triplet absorptions.

Figure 9 shows the Na–Ar RDF (solid curve) from the same simulation as described for Figure 8. The first peak occurs near 4.9 Å, very close to the minimum of the ground-state Na–Ar ($X\,^2\Sigma$) diatomic potential at 5.01 Å, and then the RDF quickly settles down to its asymptotic value of unity. The dashed curve in Figure 9 shows the Na–Ar RDF calculated for $T = 150$ K, and in the limit of zero Ar density, that is, assuming the equivalence of the Na–Ar ($X\,^2\Sigma$) diatomic potential and the potential of mean force:

$$g(R) \rightarrow \exp[-V_{\text{Na-Ar}}(R)/kT] \quad \text{as} \quad \rho_{\text{Ar}} \rightarrow 0 \quad (7)$$

The differences between the solid and dashed curves in Figure 9 indicate the importance of simultaneous multiperturber interactions in this system.

Discussion

PRELIMINARY REMARKS

The persistence of the fcc structure and the associated triplet absorption lineshape in the solid Ar simulations right up to 84 K suggests that dynamic distortion effects alone *can* account for the magnitude of triplet splittings observed experimentally for Na/Rg matrix systems.[24] Note, however, that our results do not *disprove* the hypothesis that the local structure around an M atom impurity may be amorphous, or otherwise statically disordered.

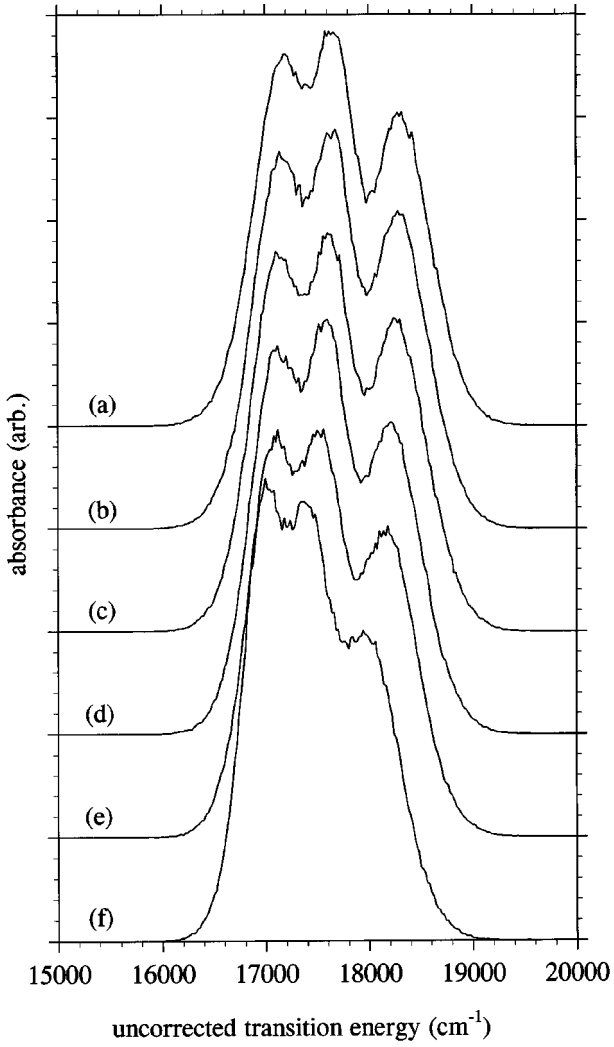

FIGURE 7. Simulated 3p ← 3s absorption spectra for a Na atom in liquid Ar at $T = 84$ K, calculated using the fcc periodic boundary conditions appropriate to the 108-atom ensemble, but with various numbers of Ar perturbers: (a) 107 Ar atoms; (b) 106 Ar atoms; (c) 105 Ar atoms; (d) 103 Ar atoms; (e) 101 Ar atoms; and (f) 94 Ar atoms. In each case, the spectra were averaged over 2.0×10^5 configurations.

As for the liquid Ar simulations, the obviously "liquid-like" nature of the Na–Ar RDFs, and the apparent insensitivity of the simulated absorption lineshapes to the observed structural artifacts [e.g., $F(\theta, \phi)$ from the 32-atom ensemble], lends confidence to our prediction of a triplet absorption lineshape for the $Na/Ar_{(l)}$ system. We will attempt a more quantitative analysis of the structural artifacts, and a more detailed comparison between experiment and simulation, below.

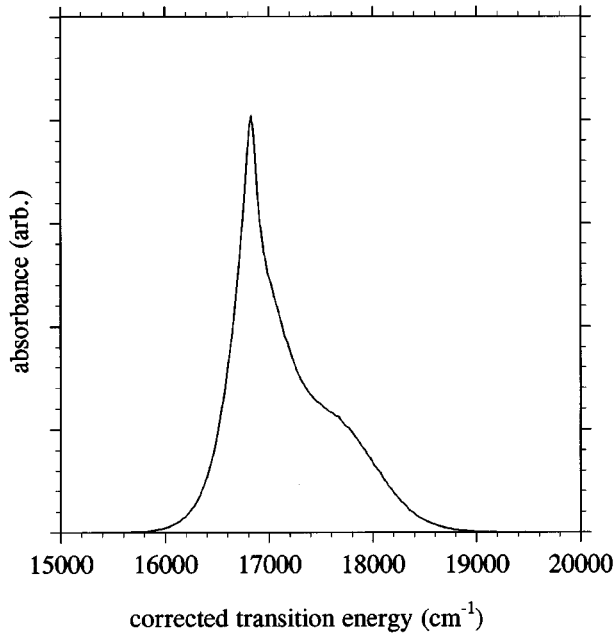

FIGURE 8. Simulated 3p ← 3s absorption spectra for a Na atom in Ar fluid at its critical point density and at $T = 150$ K, calculated using the 108-atom ensemble with fcc periodic boundary conditions, and averaged over 1.5×10^6 configurations.

FINITE-SIZE ARTIFACTS

Because the $F(\theta, \phi)$ values are calculated in a reference frame centered on the Na atom, but with a space-fixed orientation, the presence of *any*

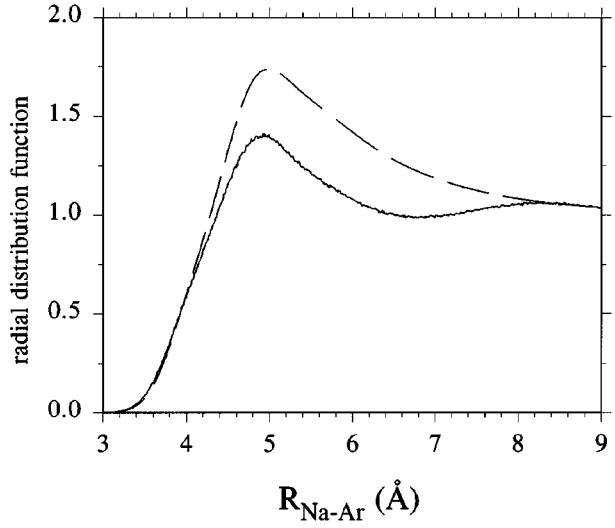

FIGURE 9. Simulated Na–Ar RDF from the calculation described in Figure 8 (solid curve). The dashed curve shows the Na–Ar RDF in the low Ar density limit calculated for $T = 150$ K using eq. (7).

structure in the data from simulations of liquid systems indicates an artificial deviation from the known isotropic nature of real liquids. Fortunately, the angular distributions in Figure 6 show a decrease in visible patterns as the size of the ensemble is increased from 32 to 108 to 256 atoms. We attempted to quantify the magnitude of these structural artifacts by expanding the simulated $F(\theta, \phi)$ in the so-called ''classical definition,'' or ''real'' spherical harmonics[25]:

$$\mathbf{Y}_{l,m}^{\text{even}}(\theta, \phi) = \sqrt{\frac{(2l+1)(l-m)!}{2\pi(l+m)!}} \times P_{l,m}[\cos(\theta)]\cos(m\phi) \quad (8)$$

in which the $P_{l,m}[\cos(\theta)]$ are associated Legendre functions, evaluated numerically using recurrence relations[26]; the $\mathbf{Y}_{l,m}^{\text{odd}}(\theta, \phi)$ are similarly defined except for the replacement of $\cos(m\phi)$ by $\sin(m\phi)$. The coefficients of the expansion of $F(\theta, \phi)$ over the even ϕ-parity real spherical harmonics are thus given by:

$$a_{l,m} = \iint F(\theta, \phi)\mathbf{Y}_{l,m}^{\text{even}}(\theta, \phi)\sin(\theta)\, d\theta\, d\phi \quad (9)$$

with a similar definition for the $b_{l,m}$ values, the coefficients of the $\mathbf{Y}_{l,m}^{\text{odd}}(\theta, \phi)$ expansion. For the solid structures depicted in Figure 3, the $a_{l,m}$ values are large for $l = 0$, 4, 6, 8, 12, 14, 16, etc. and $m = 0$, 4, 8, etc.; and the $b_{l,m}$ values are much smaller, and are nonzero only because of residual statistical errors in the simulations. Similar patterns appear in the expansion coefficients for the liquid structure simulated using the 32-atom ensemble, but only up to $l = 8$. The magnitude of these coefficients decreases with increasing ensemble size; for the 256-atom ensemble the even l value and $m = 0$, 4 pattern is still present, but barely discernible, with the magnitude of the $a_{l,m}$ values being comparable to the magnitudes of the $b_{l,m}$ values. Table III lists the magnitudes of a few selected even ϕ-parity expansion coefficients, normalized to the magnitude of the isotropic $a_{0,0}$ coefficient; that is:

$$R_{l,m} = \left|\frac{a_{l,m}}{a_{0,0}}\right| \quad (10)$$

We also note in passing that the expansion coefficients for the 141-atom ensemble in the rigid spherical box are also very small, but whether this is due to the spherical boundary conditions, or to the constant disturbances introduced by the recentering process, is unclear.

These results indicate that, even though the present spectral simulations are insensitive to the presence of these structural artifacts, future efforts at quenching liquid M/Rg ensembles to generate amorphous M/Rg solids should probably utilize even large ensembles, and/or avoid the use of periodic boundary conditions altogether.

COMPARISON WITH EXPERIMENTAL DATA

We have already commented briefly above, and in the Introduction, on the favorable comparison between the solid Ar simulations and the available matrix isolation data. Unfortunately, we know of

TABLE III.
Normalized Magnitudes of Real, Even ϕ-Parity Spherical Harmonic Expansion Coefficients for Angular Probability Distributions Shown in Figures 3 and 6.[a]

Ensemble, systems simulated	R_{40}	R_{44}	R_{80}	R_{84}	R_{88}
32-atom fcc 4 × 4 × 4 cell					
Ar liquid, T = 84 K	0.070	0.040	0.116	0.040	0.068
108-atom fcc 6 × 6 × 6 cell					
Ar solid, T = 20 K	0.398	0.236	1.089	0.420	0.626
Ar solid, T = 84 K	0.255	0.152	0.785	0.302	0.453
Ar liquid, T = 84 K	0.009	0.005	0.022	0.007	0.015
Ar fluid, T = 150 K	0.003	0.002	0.001	0.0004	0.0004
256-atom fcc 8 × 8 × 8 cell					
Ar liquid, T = 84 K	0.003	0.003	0.009	0.007	0.001
141-atom rigid spherical box					
Ar liquid, T = 84 K	0.003	0.003	0.001	0.0009	0.003

[a]The $R_{l,m}$ are calculated according to eq. (10).

no available experimental data for Na atoms in either liquid or critical-point Ar systems. However, we *have* noticed what may very well be fortuitous similarities between our simulated spectra and two other, apparently very different, experimental systems, which we feel compelled to comment on.

Figure 10a shows a comparison between a simulated $Na/Ar_{(l)}$ spectrum at $T = 84$ K (dashed curve), and an experimental absorption spectrum for a Li/Ar/Xe 50/50 host matrix at $T = 20$ K (solid curve). The similarities are striking, and probably reflect the similarities between the short-range structures present in liquids and in amorphous solids. This result also begs the question: Will there be any significant differences between the spectra calculated for liquid M/Rg systems, and those calculated as an inhomogeneous superposition of large numbers of low-temperature amorphous solid ensembles?

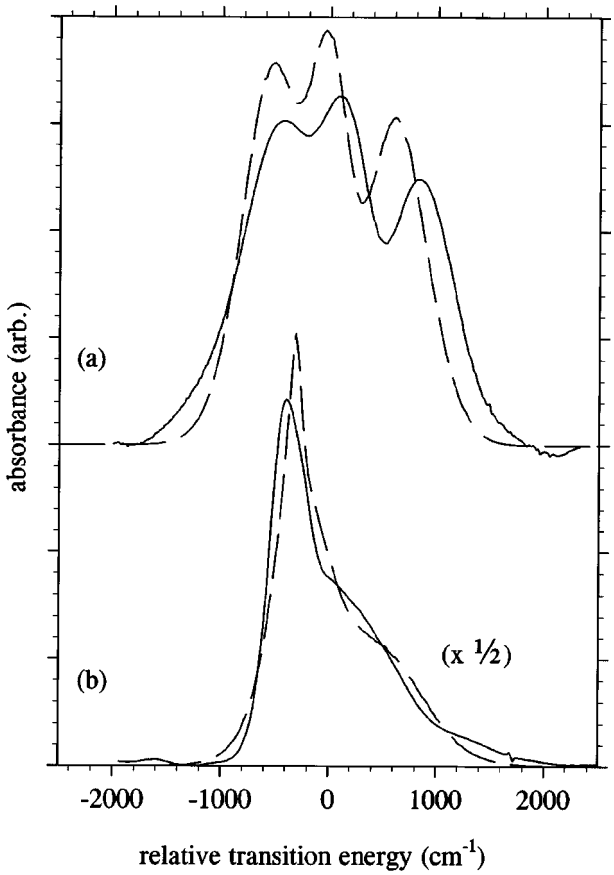

FIGURE 10. Comparison between selected simulated and experimental absorption lineshapes. The dashed curve in (a) is the result from the $Na/Ar_{(l)}$ simulation at $T = 84$ K presented in Figure 4a; the solid curve is data from mixed Ar/Xe host (50/50 composition) matrix isolation experiment on Li atoms at $T = 20$ K (data from Fig. 1e of ref. 6). The dashed curve in (b) is the result from the critical point Ar simulation shown in Figure 8; the solid curve shows the absorption of an Li/H_2 matrix at $T = 3$ K (data from Fig. 5 of ref. 10). All the spectra have been shifted to make the centroids of the absorption bands coincide, and have been normalized to the same integrated intensities, then (b) was scaled by a multiplicative factor of 1/2.

Figure 10b shows a comparison between the simulated spectrum for a Na atom in critical-point Ar fluid at $T = 150$ K, and an experimental Li/H_2 matrix spectrum taken at $T = 3$ K. Once again, the similarities are remarkable (our simulations being somewhat closer to experiment than even the results of previously published Li/H_2 simulations[27]), but in this case the underlying structural similarities are less obvious. The trend indicated by the spectral transformations shown in Figure 7, in which decreasing the Ar perturber density results in a more asymmetrical, blue-degraded lineshape, suggests a possible speculative explanation. Assuming for the moment that the Li^*-H_2 interactions are of comparable strength and range to the Na^*-Ar interactions, can some analogy be made between the radial and angular distributions of perturbers in ''quantum solid'' H_2 matrices, and in the critical Ar fluid? Perhaps the key similarity is simply a low density of multiple perturber interactions at small M–Rg distances; implying very ''loose'' trapping site structures for Li atoms in solid H_2. We have begun to pursue this issue further in a series of simulations in which we attempt to mimic ''quantum effects'' such as zero-point motion by using ''fictitious'' classical interaction potentials. Other groups have already made significant progress along similar lines,[28–30] and in defining the conditions under which the classical treatment of the nuclear coordinates implicit in eq. (1) is applicable to quantum systems such as doped H_2 matrices.[31]

Conclusions and Future Directions

The simulations of Na atoms trapped in highly statically symmetrical sites in solid Ar support the contention that the experimentally observed triplet absorption features are due to dynamic distortions of such trapping sites. We are pursuing further refinements of our lineshape model which may ultimately yield the quantitative agreement between simulation and experiment necessary to

prove this point.[32,33] We will also continue our efforts to generate model low-temperature, statically disordered systems by quenching high-temperature, dynamically disordered ensembles.

We predict a triplet absorption lineshape for Na atoms in liquid Ar, with a splitting between the outermost peaks of $\approx 1100\ cm^{-1}$ and a gas-to-liquid centroid blue shift of $\approx 600\ cm^{-1}$. We hope this information will be of use to anyone attempting an experimental study of such systems.

References

1. N. Schwentner, E. E. Koch, and J. Jortner, *Electronic Excitations in Condensed Rare Gases*, Springer, Berlin, 1985.
2. J. A. Boatz and M. E. Fajardo, *J. Chem. Phys.*, **101**, 3472 (1994).
3. L. C. Balling and J. J. Wright, *J. Chem. Phys.*, **79**, 2941 (1983).
4. K. M. Sando, G. J. Erickson, and R. C. Binning, Jr., *J. Phys. B.*, **12**, 2697 (1979).
5. P. R. Moran, *Phys. Rev.*, **137A**, 1016 (1965).
6. R. A. Corbin and M. E. Fajardo, *J. Chem. Phys.*, **101**, 2678 (1994).
7. F. F. Abraham, *J. Chem. Phys.*, **72**, 359 (1980).
8. J. D. Honeycutt and H. C. Andersen, *Chem. Phys. Lett.*, **108**, 535 (1984).
9. J. H. M. Beijersbergen, Q. Hui, and M. Takami, *Phys. Lett. A*, **181**, 393 (1993), and references therein.
10. M. E. Fajardo, *J. Chem. Phys.*, **98**, 110 (1993).
11. M. Lax, *J. Chem. Phys.*, **20**, 1752 (1952).
12. R. A. Aziz and M. J. Slaman, *Mol. Phys.*, **58**, 679 (1986).
13. R. P. Saxon, R. E. Olson, and B. Liu, *J. Chem. Phys.*, **67**, 2692 (1977).
14. C. E. Moore, *Atomic Energy Levels*, *Vol. I*, NSRDS-NBS 35, Washington, DC, 1971.
15. R. H. G. Reid and A. Dalgarno, *Phys. Rev. Lett.*, **22**, 1029 (1969).
16. C. H. Becker, P. Casavecchia, Y. T. Lee, R. E. Olson, and W. A. Lester, Jr., *J. Chem. Phys.*, **70**, 5477 (1979).
17. V. Aquilanti and G. Grossi, *J. Chem. Phys.*, **73**, 1165 (1980).
18. N. Metropolis, A. W. Rosenbluth, M. N. Rosenbluth, A. H. Teller, and E. Teller, *J. Chem. Phys.*, **21**, 1087 (1953).
19. M. P. Allen and D. J. Tildesley, *Computer Simulations of Liquids*, Oxford, New York, 1990.
20. M. E. Fajardo, *J. Chem. Phys.*, **98**, 119 (1993).
21. P. A. Egelstaff, *An Introduction to the Liquid State*, Oxford, New York, 1992.
22. P. Korpiun and E. Luscher, In *Rare Gas Solids*, *Vol. II*, M. L. Klein and J. A. Venables, Eds., Academic, London, 1976.
23. R. A. Wilsak and G. Thodos, *J. Chem. Eng. Data*, **29**, 255 (1984).
24. S. Tam and M. E. Fajardo, *J. Chem. Phys.*, **99**, 854 (1993).
25. E. Butkov, *Mathematical Physics*, Addison-Wesley, Reading, MA, 1968.
26. W. H. Press, B. P. Flannery, S. A. Teukolsky, and W. T. Vetterling, *Numerical Recipes*, Cambridge University Press, Cambridge, 1989.
27. D. Scharf, G. J. Martyna, D. Li, G. A. Voth, and M. L. Klein, *J. Chem. Phys.*, **99**, 9013 (1993).
28. G. A. Voth, Quantum simulations of potential high energy density materials, In *Proceedings of the High Energy Denstiy Matter (HEDM) Contractors' Conference, 4–7 June 1995, Woods Hole, MA*, P. G. Carrick and S. Tam, Eds., PL-TR-95-3039, Edwards AFB, CA, 1995.
29. M. Pavese and G. A. Voth, *Chem. Phys. Lett.*, **249**, 231 (1996).
30. Z. Li, M. Sterling, and V. A. Apkarian, Simulations of quantum many-body systems by classical dynamics, In *Proceedings of the High Energy Density Matter (HEDM) Contractors' Conference, 4–7 June 1995, Woods Hole, MA*, P. G. Carrick and S. Tam, Eds., PL-TR-95-3039, Edwards AFB, CA, 1995.
31. W. G. Lawrence and V. A. Apkarian, *J. Chem. Phys.*, **101**, 1820 (1994).
32. P. W. Langhoff, J. A. Boatz, and M. E. Fajardo, Theoretical methods for cryogenically trapped metal radical spectra, In *Proceedings of the High Energy Density Matter (HEDM) Contractors' Conference, 5–7 June 1994, Crystal Bay, NV*, T. L. Thompson and S. L. Rodgers, Eds., PL-TR-94-3036, Edwards AFB, CA, 1994.
33. P. W. Langhoff, *J. Phys. Chem.*, **100**, 2974 (1996).